IEEE Robotics and Automation Letters (RA-L) paper, presented at ICRA 2024, Yokohama, Japan. Cite as RA-L paper.

Investigating Stability Outcomes Across Diverse Gait Patterns in Quadruped Robots: A Comparative Analysis

Zhongjin Ju[1], *Graduate Student Member, IEEE*, Ke Wei[1], *Student Member, IEEE*, Lei Jin[1], Yundou Xu[1,2,*], *Member, IEEE*

***Abstract*—Quadruped robots have gained attention for their potential to navigate various terrains. However, the stability of these robots in different gait sequences remains an open question. This study investigates the relationship between different gait sequences and the motion stability of quadruped robots, assuming a flat terrain for the purpose of the analysis. Utilizing mathematical models based on spiral theory, we examine the stability margins associated with different leg movement sequences. Notably, our findings confirm that the most commonly observed sequence in both natural and robotic contexts indeed offers optimal stability. The study also scrutinizes the influence of the robot's structural parameters and gait configuration on its motion stability. These results provide a theoretical foundation for the design and stability control of quadruped robots, setting the stage for future work on more complex terrains.**

***Index Terms*—Quadruped, Stability analysis, Gait analysis, Screw theory, Biomimetic.**

I. Introduction

QUADRUPEDAL locomotion, a form of movement observed in approximately 5,400 species of mammals and an increasing variety of robots [1], poses compelling questions about the interplay between gait sequence and stability. Despite the diversity of potential gait patterns, certain sequences are predominantly observed both in nature and in robotic applications [2]. However, the underlying reasons for the preference for these specific gait sequences remain underexplored. Our research narrows this gap by investigating the stability margins of six different gait sequences in quadruped robots. The aim is to elucidate the mechanisms that could make certain sequences more stable than others, thereby providing guidelines for the design of more robust quadruped robots.

Quadruped robots have seen significant evolution, from early bio-inspired designs to highly sophisticated systems like Boston Dynamics' Spot robot [3], Stanford Doggo [4], and others [5]–[7]. Among the first to propose stability criteria for quadruped robots was McGhee, who suggested six gaits designed to maintain at least three legs in contact with the ground during motion [8]. Subsequent research has largely been focused on these foundational gaits [9]–[13].

Existing studies have emphasized the importance of stability in crawing gaits [14]–[17] and employed Particle Swarm Optimization (PSO) algorithms for optimizing stability margins [18]. However, there is limited work that systematically compares the stability across different gait sequences. This paper advances the field by offering a comprehensive stability analysis for six different gait sequences, some of which have been partially optimized using PSO [19], [20].

While various methodologies have been employed to enhance the stability of quadruped robots on uneven terrains [21]–[30], few have rigorously explained why certain gaits are predominantly used over others in either natural or robotic quadrupeds.

Our research addresses a gap in the field by analyzing stability margins across multiple gait sequences and investigating why the most observed sequence—right front leg, left hind leg, right hind leg, left front leg—is often preferred in both biological and robotic contexts. The goal is to guide future quadruped robotics by systematically evaluating the stability margins of various gait sequences. The key contributions of this study are:

1) An initial theoretical analysis using spiral theory to assess the stability margins of six different gait sequences, providing a preliminary understanding of which sequences may offer superior stability.

2) Experimental analyses of six different gait sequences to evaluate their motion performance, offering a comprehensive view of their effectiveness and stability.

3) Analysis and comparison of the stability of different gait sequences during the stride planning of quadruped robots, using stability margin results, body oscillation amplitudes, and yaw angles.

This paper focuses on the assumption that quadruped robots operate on flat terrains, allowing for a controlled study of gait sequences and their influence on stability. However, this assumption limits the consideration of the adaptability of quadruped robots to more complex terrains.

II. Influence of Movement Sequences on Motion during Crawling Gait

In this section, we calculate the stability margins for different gait sequences in quadruped robots using screw theory. A

*This document is the results of the research project funded by National Natural Science Foundation of China (Grant No. 51875495).

*Corresponding author

[1]Parallel Robot and Mechatronic System Laboratory of Hebei Province, Yanshan University, Qinhuangdao, 066004.

[2]Key Laboratory of Advanced Forging and Stamping Technology and Science (Yanshan University), Ministry of Education of China, Qinhuangdao, 066004.

IEEE Robotics and Automation Letters (RA-L) paper, presented at ICRA 2024, Yokohama, Japan. Cite as RA-L paper.

IEEE Robotics and Automation Letters (RA-L) paper, presented at ICRA 2024, Yokohama, Japan. Cite as RA-L paper.

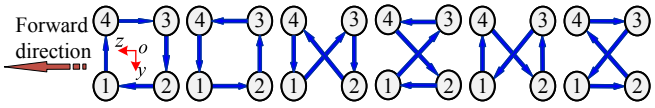

Fig. 1. The six different sequences crawl gait of quadruped robot.

TABLE I
SUMMARY OF VARIABLES AND DEFINITIONS

Variable	Definition (Note: All variables and parameters are dimensionless.)
$o(\boldsymbol{G})$	Projection of the robot's body mass onto the plane formed by the feet. Assumption: The robot's body is homogenous and completely symmetrical, and the ground under consideration is flat. Therefore, the position of $o(\boldsymbol{G})$ relative to the robot's body remains constant.
T	Time duration of a single gait cycle.
t_β	Time duration of the support phase within a single gait cycle.
v	Velocity of the robot during the support phase.
δ	Half of the robot's body width, a constant design parameter.
β	Support distance, representing the length traversed by the supporting feet during the support phase. β_i refers specifically to the support distance of leg i. β is a variable that can change during a gait cycle and is influenced by the robot's leg length and joint angles. Specifically, $\beta = v \cdot t_\beta$.
t_{ϕ_i}	Time interval between the footfall of leg i relative to the footfall of leg 1 during a gait cycle.
ϕ_i	A distance that satisfies $\phi_i = \beta \cdot t_{\phi_i} / t_\beta$.
a	Foot distance. Distance from the robot's midplane to either the lift-off point for front legs or the footfall point for rear legs. Under the assumption that the robot's body is homogenous, this distance is considered to be the same for both lift-off and footfall points and is denoted by a. In cases where one leg is lifting off and the other is touching down on the same side of the body, the distance between the two legs is $2a$. Variable a is inversely related to β.
(γ_i, δ_i)	Coordinate of the footfall point for leg i, relative to the origin $o(G)$, within a single gait cycle. Here, δ_i is equal to the body width δ, and its sign is determined by which side of the body the leg is on. Note that these coordinates specify only the point where the foot makes initial contact with the ground.
Ψ	Stability margin defined as the minimum distance from the projected center of mass to each of the three sides of the support region.
$\Psi_{\min}$	Minimum stability margin occurring at an instant during a gait cycle.
$\Psi_{\max}$	Maximum stability margin occurring at an instant during a gait cycle.
Ψ_{avg}	Average stability margin calculated over all instants in a gait cycle.
$S_\triangle$	Represents the size of the support region, defined as the area of the triangle formed by the supporting feet.
$S_{\triangle\,\min}$	Minimum area of the support region during a gait cycle.
$S_{\triangle\,\max}$	Maximum area of the support region during a gait cycle.
H_0	Represents the maximum step height for each leg, measured as the maximum distance from the ground to the tip of the foot during the step cycle.

quadruped robot has a total of $A_4^3 = 24$ unique combinations for moving its legs in different sequences. However, given the structural symmetry of the robot, any leg can serve as the initial leg in the sequence, effectively reducing the number of unique sequences to $\frac{A_4^3}{4} = 6$. These unique sequences are: 1-4-3-2-1, 1-2-3-4-1, 1-3-2-4-1, 1-3-4-2-1, 1-4-2-3-1, and 1-2-4-3-1. These sequences are further illustrated in Fig. 1.

The key variables and parameters for our study are shown in Table I, with some parameters further elaborated in Fig. 2.

Definition 1: The *gait matrix*, denoted by $\boldsymbol{K}$, is a 4×4 matrix where each row characterizes a specific feature of a

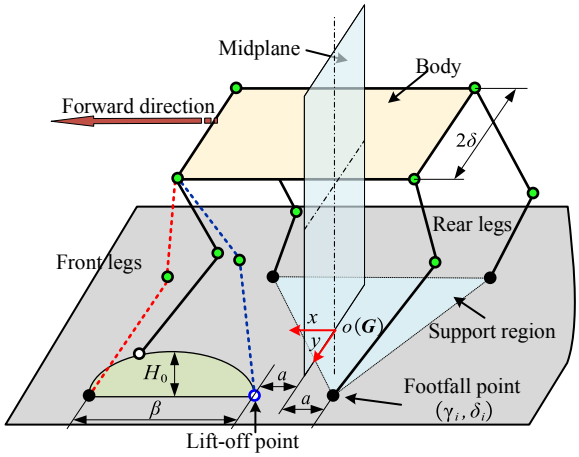

Fig. 2. Definition of Variables and Parameters for Gait Analysis.

quadruped robot's gait. The matrix is formally defined as:

$$\boldsymbol{K} = \begin{bmatrix} \beta_1 & \beta_2 & \beta_3 & \beta_4 \\ \gamma_1 & \gamma_2 & \gamma_3 & \gamma_4 \\ \delta_1 & \delta_2 & \delta_3 & \delta_4 \\ 0 & \phi_2 & \phi_3 & \phi_4 \end{bmatrix}. \tag{1}$$

- The first row, β_i, represents the maximum support distance for foot 1.
- The second row, γ_i, and the third row, δ_i, indicate the coordinates of the footfall positions for foot i.
- The fourth row, ϕ_i (for $i \neq 1$), shows the remaining distance foot i needs to cover to touch down when foot 1 has just landed. If each leg moves at a constant and equal speed, this row provides information about both the sequence of leg movements and the timing of the swing phase.

Here, $\boldsymbol{K}$ encapsulates both the spatial and temporal elements of the quadruped's gait in a concise manner. It also provides an instantaneous snapshot of the positions of each foot within the gait cycle, including the order in which they move.

To facilitate the study of how different step sequences affect the robot's locomotion performance, we standardize the gait parameters across various sequences. Specifically, the supporting distance β and the foot distance a are maintained consistently. In this standardized setting, a leg sequence and its accompanying parameters can be denoted by $\boldsymbol{K}_{seq}$, such as $\boldsymbol{K}_{1342}$ given by:

$$\boldsymbol{K}_{1342} = \begin{bmatrix} \beta & \beta & \beta & \beta \\ \beta + a & -a & -a & \beta + a \\ \delta & \delta & -\delta & -\delta \\ 0 & \beta & \frac{\beta}{3} & \frac{2\beta}{3} \end{bmatrix}. \tag{2}$$

Although the leg sequence is already encapsulated in the columns of $\boldsymbol{K}$, we include the subscript $\{1342\}$ to make the sequence explicit

As shown in Fig. 3, the distribution of the supporting feet when a quadruped robot adopts the $\boldsymbol{K}_{1342}$ gait and leg 4 is just lifting off the ground. In the figure, the screw $\$^{ij}$ represents the helix of foot j relative to foot i in space. η_1, η_2, and η_3 are the shortest distances from the center of mass to the three sides.

IEEE Robotics and Automation Letters (RA-L) paper, presented at ICRA 2024, Yokohama, Japan. Cite as RA-L paper.

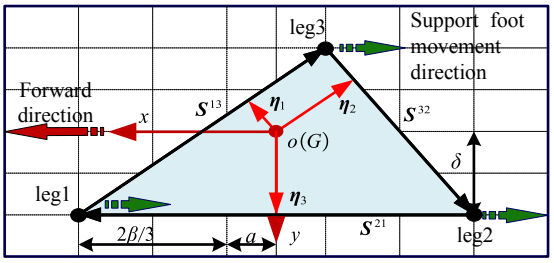

Fig. 3. Touch-down point and geometric parameters of support legs.

From Fig. 3, the coordinates of the supporting feet at this instant can be expressed as:

$$\begin{bmatrix} \boldsymbol{leg1} \\ \boldsymbol{leg2} \\ \boldsymbol{leg3} \end{bmatrix} = \begin{bmatrix} \frac{2\beta}{3}+a & \delta & z_1 \\ \frac{-2\beta}{3}-a & \delta & z_2 \\ -a & -\delta & z_3 \end{bmatrix}. \tag{3}$$

Subsequently, the Plücker coordinates and the screw of the supporting feet at this instant can be represented as:

$$\begin{bmatrix} \$^{13} \\ \$^{32} \\ \$^{21} \end{bmatrix} = \begin{bmatrix} (\boldsymbol{S}^{13}; \boldsymbol{S}_0^{13}) \\ (\boldsymbol{S}^{32}; \boldsymbol{S}_0^{32}) \\ (\boldsymbol{S}^{21}; \boldsymbol{S}_0^{21}) \end{bmatrix}, \tag{4}$$

whrer, $\boldsymbol{S}^{ij}$ is the real unit of the $\$^{13}$; $\boldsymbol{S}_0^{ij}$ is the dual unit of the $\$^{13}$.

As shown in Fig. 3, when all supporting feet are on the same horizontal plane, there are:

$$\begin{bmatrix} \boldsymbol{S}^{13} \\ \boldsymbol{S}^{32} \\ \boldsymbol{S}^{21} \end{bmatrix} = \begin{bmatrix} \frac{-2\beta}{3}-2a & -2\delta & 0 \\ \frac{-2\beta}{3} & 2\delta & 0 \\ \frac{4\beta}{3}+2a & 0 & 0 \end{bmatrix}. \tag{5}$$

The real unit and dual unit satisfy the cross product rule, which is $\boldsymbol{S}_0^{ij} = \boldsymbol{leg}i \times \boldsymbol{S}^{ij}$. So,

$$\begin{bmatrix} \boldsymbol{S}_0^{13} \\ \boldsymbol{S}_0^{32} \\ \boldsymbol{S}_0^{21} \end{bmatrix} = \begin{bmatrix} 0 & 0 & \frac{-2\beta\delta}{3} \\ 0 & 0 & -2\delta a - \frac{2\beta\delta}{3} \\ 0 & 0 & \frac{-4\beta\delta}{3} - 2\delta a \end{bmatrix}. \tag{6}$$

The minimum distance from the center of mass projected onto the three side lines satisfies that vector $\boldsymbol{\eta_1}$ is orthogonal to $\$^{13}$, vector $\boldsymbol{\eta_2}$ is orthogonal to $\$^{32}$, and vector $\boldsymbol{\eta_3}$ is orthogonal to $\$^{21}$, that is:

$$\begin{bmatrix} \boldsymbol{\eta}_1 \times \boldsymbol{S}^{13} \\ \boldsymbol{\eta}_2 \times \boldsymbol{S}^{32} \\ \boldsymbol{\eta}_3 \times \boldsymbol{S}^{21} \end{bmatrix} = \begin{bmatrix} \boldsymbol{S}_0^{13} \\ \boldsymbol{S}_0^{32} \\ \boldsymbol{S}_0^{21} \end{bmatrix}. \tag{7}$$

Take the cross product of both sides of (7) with their respective real units, that is,

$$\begin{bmatrix} \boldsymbol{S}^{13} \times (\boldsymbol{\eta}_1 \times \boldsymbol{S}^{13}) \\ \boldsymbol{S}^{32} \times (\boldsymbol{\eta}_2 \times \boldsymbol{S}^{32}) \\ \boldsymbol{S}^{21} \times (\boldsymbol{\eta}_3 \times \boldsymbol{S}^{21}) \end{bmatrix} = \begin{bmatrix} \boldsymbol{S}^{13}\boldsymbol{S}^{13}\boldsymbol{\eta}_1 - \boldsymbol{S}^{13}\boldsymbol{\eta}_1\boldsymbol{S}^{13} \\ \boldsymbol{S}^{32}\boldsymbol{S}^{32}\boldsymbol{\eta}_2 - \boldsymbol{S}^{32}\boldsymbol{\eta}_2\boldsymbol{S}^{32} \\ \boldsymbol{S}^{21}\boldsymbol{S}^{21}\boldsymbol{\eta}_3 - \boldsymbol{S}^{21}\boldsymbol{\eta}_3\boldsymbol{S}^{21} \end{bmatrix}. \tag{8}$$

The vector of the center of mass projected onto the three sides are obtained by combining (7) and (8).

$$\begin{bmatrix} \boldsymbol{\eta}_1 \\ \boldsymbol{\eta}_2 \\ \boldsymbol{\eta}_3 \end{bmatrix} = \begin{bmatrix} \frac{\boldsymbol{S}^{13} \times \boldsymbol{S}_0^{13}}{\boldsymbol{S}^{13} \cdot \boldsymbol{S}^{13}} \\ \frac{\boldsymbol{S}^{32} \times \boldsymbol{S}_0^{32}}{\boldsymbol{S}^{32} \cdot \boldsymbol{S}^{32}} \\ \frac{\boldsymbol{S}^{21} \times \boldsymbol{S}_0^{21}}{\boldsymbol{S}^{21} \cdot \boldsymbol{S}^{21}} \end{bmatrix}. \tag{9}$$

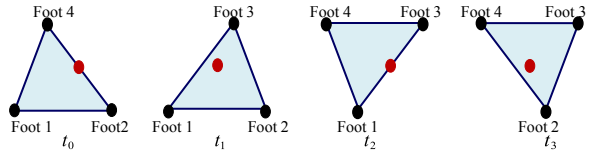

Fig. 4. The changing sequence of supporting legs during the $\boldsymbol{K}_{1342}$ gait.

TABLE II
COORDINATE CHANGES OF EACH FOOT DURING A $\boldsymbol{K}_{1342}$ GAIT CYCLE

F_i	t_0	t_1	t_2	t_3
F_1	$\begin{bmatrix} \beta+a \\ \delta \\ 0 \end{bmatrix}$	$\begin{bmatrix} \frac{2\beta}{3}+a \\ \delta \\ 0 \end{bmatrix}$	$\begin{bmatrix} \frac{\beta}{3}+a \\ \delta \\ 0 \end{bmatrix}$	$\begin{bmatrix} a \\ \delta \\ 0 \end{bmatrix}$
F_2	$\begin{bmatrix} \frac{-\beta-3a}{3} \\ \delta \\ 0 \end{bmatrix}$	$\begin{bmatrix} \frac{-2\beta-3a}{3} \\ \delta \\ 0 \end{bmatrix}$	$\begin{bmatrix} -\beta-a \\ \delta \\ 0 \end{bmatrix}$	$\begin{bmatrix} -a \\ \delta \\ 0 \end{bmatrix}$
F_3	$\begin{bmatrix} -\beta-a \\ -\delta \\ 0 \end{bmatrix}$	$\begin{bmatrix} -a \\ -\delta \\ 0 \end{bmatrix}$	$\begin{bmatrix} \frac{-\beta-3a}{3} \\ -\delta \\ 0 \end{bmatrix}$	$\begin{bmatrix} \frac{-2\beta-3a}{3} \\ -\delta \\ 0 \end{bmatrix}$
F_4	$\begin{bmatrix} \frac{\beta}{3}+a \\ -\delta \\ 0 \end{bmatrix}$	$\begin{bmatrix} a \\ -\delta \\ 0 \end{bmatrix}$	$\begin{bmatrix} \beta+a \\ -\delta \\ 0 \end{bmatrix}$	$\begin{bmatrix} \frac{2\beta+3a}{3} \\ -\delta \\ 0 \end{bmatrix}$

Take the modulus of (9) to obtain the minimum distances from the center of mass projected onto each of the three sides:

$$\begin{bmatrix} \eta_1 \\ \eta_2 \\ \eta_3 \end{bmatrix} = \begin{bmatrix} \delta\beta\left(\beta^2+9\delta^2+9a^2+6a\beta\right)^{-\frac{1}{2}} \\ \delta\left(\beta+3a\right)\left(\beta^2+9\delta^2\right)^{-\frac{1}{2}} \\ \delta \end{bmatrix}. \tag{10}$$

For a quadruped robot, the stability margin at each moment should be the shortest distance from the projection of the center of mass (COM) to the triangle formed by the three supporting feet, i.e.,

$$\Psi = \min\left(\eta_1, \eta_2, \eta_3\right) \tag{11}$$

Therefore, in the state shown in Fig .3, the stability margin $\Psi = \eta_1$. However, the gait cycle of a quadruped robot is a continuous process, with the supporting feet changing over time. As shown in Fig .4, it is a diagram illustrating the change in the entire support region during the $\boldsymbol{K}_{1342}$ gait.

In the entire $\boldsymbol{K}_{1342}$ gait cycle, as shown in Fig .4, the coordinate changes of the feet are shown in Table II, where F_i is an abbreviation for Foot i.

Based on the coordinate changes in the $\boldsymbol{K}_{1342}$ gait cycle shown in Table II, and combining equations (4) to (10), the distance between the projection of the center of mass and the supporting edge when each leg touches and leaves the ground during the $\boldsymbol{K}_{1342}$ gait cycle can be obtained. Table III shows the values of the distance between the projection of the center of mass and the supporting boundary when each leg touches and leaves the ground in the $\boldsymbol{K}_{1342}$ gait cycle, where l_{ij} represents the boundary formed by foot i and foot j. lf_- represents that the foot is on the verge of lifting off but has not yet left the ground. lf_+ represents that the foot has just lifted off the ground.

In Table III, the minimum stability margin $\Psi_{\min}$ and the average stability margin Ψ_{avg} during the K_{1342} gait cycle can be determined as follows:

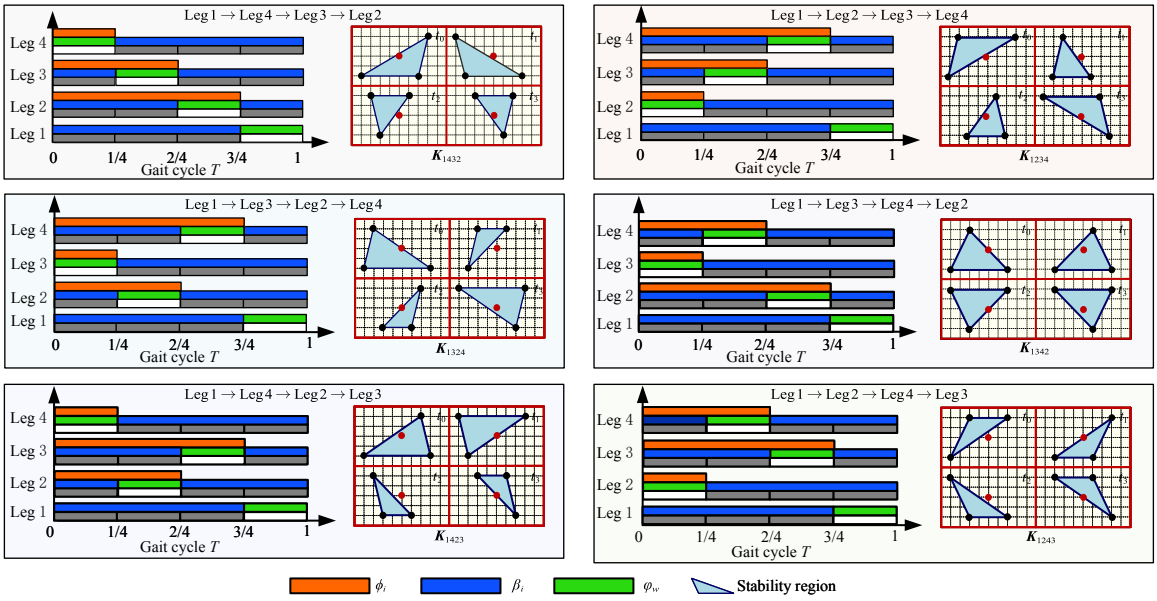

Fig. 5. Six different gait sequences and sequence diagrams of quadruped robot.

TABLE III
DISTANCE OF THE CENTER OF GRAVITY PROJECTION FROM EACH SUPPORTING SIDE DURING TOUCH-DOWN AND TAKE-OFF IN A $\boldsymbol{K}_{1342}$ GAIT CYCLE

Time	l_{13}	l_{32}	l_{21}	Ψ
t_{0+}, lf$_+$	$\frac{\delta(2\beta+3a)}{\sqrt{\beta^2+9\delta^2}}$	0	δ	0
t_{1-}, lf$_-$	$\frac{\delta(\beta+3a)}{\sqrt{\beta^2+9\delta^2}}$	$\frac{\delta\beta}{\sqrt{9\delta^2+(3a+\beta)^2}}$	δ	$\frac{\delta\beta}{\sqrt{9\delta^2+(3a+\beta)^2}}$
t_{1+}, lf$_+$	$\frac{\delta\beta}{\sqrt{9\delta^2+(3a+\beta)^2}}$	$\frac{\delta(\beta+3a)}{\sqrt{\beta^2+9\delta^2}}$	δ	$\frac{\delta\beta}{\sqrt{9\delta^2+(3a+\beta)^2}}$
t_{2-}, lf$_-$	0	$\frac{\delta(2\beta+3a)}{\sqrt{\beta^2+9\delta^2}}$	δ	0
t_{2+}, lf$_+$	$\frac{\delta(2\beta+3a)}{\sqrt{\beta^2+9\delta^2}}$	δ	0	0
t_{3-}, lf$_-$	$\frac{\delta(\beta+3a)}{\sqrt{\beta^2+9\delta^2}}$	δ	$\frac{\delta\beta}{\sqrt{9\delta^2+(3a+\beta)^2}}$	$\frac{\delta\beta}{\sqrt{9\delta^2+(3a+\beta)^2}}$
t_{3+}, lf$_+$	$\frac{\delta\beta}{\sqrt{9\delta^2+(3a+\beta)^2}}$	δ	$\frac{\delta(\beta+3a)}{\sqrt{\beta^2+9\delta^2}}$	$\frac{\delta\beta}{\sqrt{9\delta^2+(3a+\beta)^2}}$
t_{4-}, lf$_-$	0	δ	$\frac{\delta(2\beta+3a)}{\sqrt{\beta^2+9\delta^2}}$	0

$$\Psi_{\min} = 0, \tag{12}$$

$$\Psi_{avg} = \frac{\delta\beta}{2\sqrt{9\delta^2+(3a+\beta)^2}}. \tag{13}$$

As shown in Fig .1, there are six different crawling gaits for the quadruped robot, and their respective supporting domain changes and time sequences are illustrated in Fig .5.

Combining Fig .5 and the above analysis process, the minimum stability margin and average stability margin values when a quadruped robot moves in six different gait sequences can be obtained. The results are shown in Table IV.

From Table IV, it can be seen that although the quadruped robot can achieve the maximum stability margin $\Psi_{\max} = \delta\beta\left(\delta^2+(3a+\beta)^2\right)^{-1/2}$ when adopting the $\boldsymbol{K}_{1324}$ gait, when the quadruped robot adopts the $\boldsymbol{K}_{1342}$ gait, its minimum stability margin value $\Psi_{\min} = 0$ is the largest among the six gaits. In addition, the average stability margin $\Psi_{\text{avg}} = 2\delta\beta\left(9\delta^2+(3a+\beta)^2\right)^{-1/2}$ of the $\boldsymbol{K}_{1342}$ gait is also the largest among the six stability margins. Similarly, although the $\boldsymbol{K}_{1324}$ and $\boldsymbol{K}_{1423}$ gaits have relatively large maximum support areas $S_{\Delta\max}$, their minimum support areas are both smaller than the minimum support area of the $\boldsymbol{K}_{1342}$ gait. Moreover, the support area of the $\boldsymbol{K}_{1342}$ gait sequence does not vary much throughout the entire gait cycle, whereas the support areas of the other gaits vary widely, which is not conducive to the stable movement of the quadruped robot.

In this study, we consider the minimum stability margin $\Psi_{\min}$ to be the most critical indicator, as it reflects the performance of the quadruped robot in the most unstable situations. A lower minimum stability margin $\Psi_{\min}$ implies that the robot may not be able to maintain balance in certain gaits. Therefore, focusing on the minimum stability margin $\Psi_{\min}$ when designing and optimizing gaits can ensure that the robot remains stable under various conditions. However, the maximum stability margin $\Psi_{\max}$ also has certain importance, as it reflects the stability of the robot under optimal conditions. Although this indicator may not be as important as $\Psi_{\min}$ in some cases, it can still provide researchers with information about the potential stability of the robot. In some application scenarios, such as experiments conducted in controlled environments, the $\Psi_{\max}$ may be more valuable. In addition, the Ψ_{avg} provides an overview of the overall stability of the robot. It can help researchers understand the average performance of the robot under various conditions. In tasks where overall performance needs to be focused on, the average stability margin may be more important.

III. EXPERIMENT AND DISCUSSION

The experimental prototype for this study is the Unitree A1 quadruped robot, as shown in Fig. 6. The quadruped robot was tested with the six gaits shown in Fig. 5, following a

IEEE Robotics and Automation Letters (RA-L) paper, presented at ICRA 2024, Yokohama, Japan. Cite as RA-L paper.

TABLE IV
MINIMUM AND AVERAGE STABILITY MARGINS OF QUADRUPED ROBOT WITH DIFFERENT MOVING ORDERS

Gaits	$\Psi_{\min}$	$\Psi_{\max}$	Ψ_{avg}	$S_{\Delta\,\min}$	$S_{\Delta\,\max}$
$\boldsymbol{K}_{1432}$	$\frac{-\delta\beta}{\sqrt{36\delta^2+(6a+\beta)^2}}$	$\frac{\delta\beta}{\sqrt{36\delta^2+(6a+\beta)^2}}$	0	$\delta\left(2a+\frac{2\beta}{3}\right)$	$\delta\left(2a+\frac{4\beta}{3}\right)$
$\boldsymbol{K}_{1234}$	$\frac{-\delta(6a+\beta)}{\sqrt{\beta^2+36\delta^2}}$	$\frac{\delta\beta}{\sqrt{36\delta^2+(6a+\beta)^2}}$	$\frac{\beta\delta}{\sqrt{36\delta^2+(6a+\beta)^2}}-\frac{\delta(6a+\beta)}{\sqrt{\beta^2+36\delta^2}}$	$\delta\left(2a+\frac{2\beta}{3}\right)$	$\delta\left(2a+\frac{4\beta}{3}\right)$
$\boldsymbol{K}_{1324}$	$\frac{-\delta\beta}{\sqrt{\delta^2+(3a+\beta)^2}}$	$\frac{\delta\beta}{\sqrt{\delta^2+(3a+\beta)^2}}$	0	$\delta\left(2a+\frac{\beta}{3}\right)$	$\delta\left(2a+\frac{5\beta}{3}\right)$
$\boldsymbol{K}_{1342}$	0	$\frac{\delta\beta}{\sqrt{9\delta^2+(3a+\beta)^2}}$	$\frac{2\delta\beta}{\sqrt{9\delta^2+(3a+\beta)^2}}$	$\delta\left(2a+\frac{4\beta}{3}\right)$	$\delta\left(2a+\frac{4\beta}{3}\right)$
$\boldsymbol{K}_{1423}$	$\frac{-\delta\beta}{\sqrt{9\delta^2+(3a+\beta)^2}}$	$\frac{\delta\beta}{\sqrt{9\delta^2+(3a+2\beta)^2}}$	0	$\delta\left(2a+\frac{\beta}{3}\right)$	$\delta\left(2a+\frac{5\beta}{3}\right)$
$\boldsymbol{K}_{1243}$	$\frac{-\delta\beta}{\sqrt{9\delta^2+(3a+2\beta)^2}}$	0	$\frac{-2\delta\beta}{\sqrt{9\delta^2+(3a+2\beta)^2}}$	$\delta\left(2a+\frac{2\beta}{3}\right)$	$\delta\left(2a+\frac{2\beta}{3}\right)$

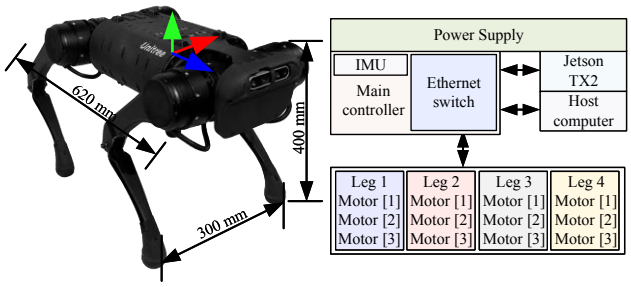

Fig. 6. Experimental prototype.

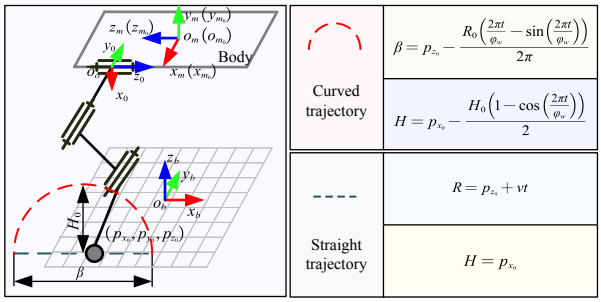

Fig. 7. Foot trajectory.

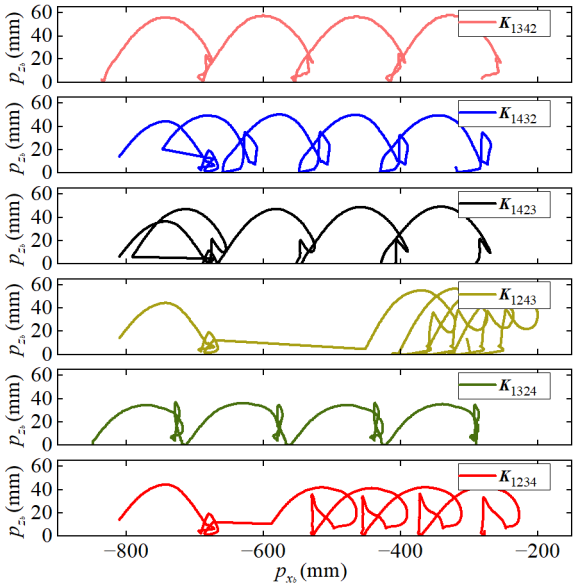

Fig. 8. Comparison of foot trajectories.

certain foot trajectory and a certain moving speed (40 mm/s). The expected foot trajectory is shown in Fig. 7, where H_0 = 60 mm and β = 100 mm. In Fig. 7, the frames o_b-$x_by_bz_b$ and o_{m_0}-$x_{m_0}y_{m_0}z_{m_0}$ are fixed coordinate systems, while the frames o_0-$x_0y_0z_0$ and o_m-$x_my_mz_m$ are affixed to the body of the quadruped robot, moving along with it. p_{x_b}, p_{y_b} and p_{z_b} are position coordinates relative to the frame o_b-$x_by_bz_b$; p_{x_0}, p_{y_0} and p_{z_0} are position coordinates relative to the frame o_0-$x_0y_0z_0$; $p_{x_{m_0}}$, $p_{y_{m_0}}$ and $p_{z_{m_0}}$ are position coordinates relative to the frame o_{m_0}-$x_{m_0}y_{m_0}z_{m_0}$.

A. Gait Trajectory Comparison

We utilized the same foot trajectory (as shown in Fig. 8) and the same position control mode (i.e., sending foot trajectory points every 1 ms to complete a trajectory motion within 250 ms) to test the motion performance under different step sequences.

Fig. 8 illustrates the foot trajectory curve of foot 1 under different step sequences. As can be seen from Fig. 8, among the six step sequences, the step height of the $\boldsymbol{K}_{1342}$ is the highest. This validates the previous statement that a negative $\Psi_{\min}$ could potentially destabilize the robot's center of gravity, causing the robot's foot to touch the ground prematurely due to the tilt of the body. This is reflected in the foot trajectory as a step height less than the expected value (H_0 = 60 mm). Although the $\Psi_{\min}$ of $\boldsymbol{K}_{1243}$ is greater than that of $\boldsymbol{K}_{1423}$, the $\Psi_{\max}$ of $\boldsymbol{K}_{1243}$ is less than that of $\boldsymbol{K}_{1423}$, resulting in the trajectory effect of $\boldsymbol{K}_{1423}$ being superior to that of $\boldsymbol{K}_{1243}$. This indicates that under the premise of the same $\Psi_{\min}$, the $\Psi_{\max}$ also plays a certain role in the foot trajectory. Although the step height of $\boldsymbol{K}_{1324}$ is far less than the ideal height (the maximum height is only 40 mm), the trajectory curve in the figure shows that the trajectory of $\boldsymbol{K}_{1324}$ is more regular than that of $\boldsymbol{K}_{1234}$, $\boldsymbol{K}_{1243}$, and $\boldsymbol{K}_{1423}$. This may be due to the $\Psi_{\max}$ of $\boldsymbol{K}_{1324}$ being the largest among the six gaits. In summary, the $\Psi_{\min}$ has the greatest impact on the step height of the foot trajectory, and the $\Psi_{\max}$ has the greatest interference with the trajectory, in other words, we can use Ψ_{avg} to judge the stability effect.

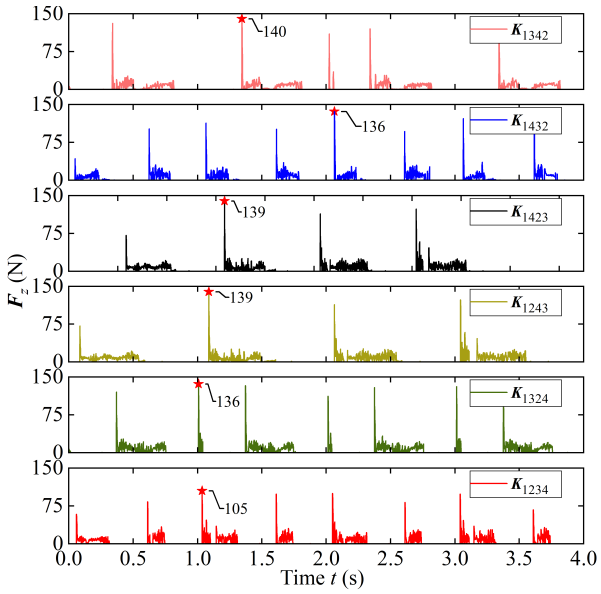

Fig. 9. Impact force curves for six different gaits.

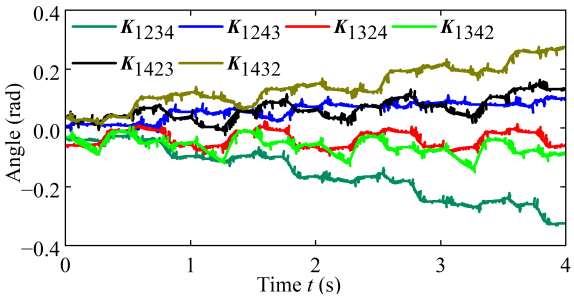

Fig. 10. Effect of Gait on Yaw Angle.

B. Comparison of Foot Impact Forces

The focus of this subsection is to compare the impact forces experienced by foot 1 under six different gait conditions. Fig. 9 depicts the impact force curves under these six distinct gaits.

We conducted six tests for each robotic gait under identical conditions to ascertain the average impact force experienced by each leg, as depicted in Table V. (i.e., the average impact force received by each foot, where Foot$_{avg}$represents the average of the total impact force received by all legs.)

TABLE V
AVERAGE IMPACT FORCE RECEIVED BY EACH FOOT IN DIFFERENT GAITS.

Gait	Foot 1	Foot 2	Foot 3	Foot 4	Foot$_{avg}$	$\Psi_{\min}$	$\Psi_{\max}$	Ψ_{avg}
$\boldsymbol{K}_{1342}$	3.82	3.52	3.59	5.87	16.80	0	29.24	58.48
$\boldsymbol{K}_{1432}$	3.88	4.28	3.84	4.49	16.49	-15.62	15.62	0
$\boldsymbol{K}_{1243}$	4.57	3.28	5.35	3.64	16.84	-25.61	0	-51.21
$\boldsymbol{K}_{1423}$	2.97	3.40	4.89	5.06	16.32	-29.24	25.61	0
$\boldsymbol{K}_{1324}$	4.20	4.48	3.98	4.02	16.68	-40.36	40.36	0
$\boldsymbol{K}_{1234}$	4.15	4.02	4.69	3.65	16.51	-118.95	15.62	-103.33

TABLE VI
CORRELATION COEFFICIENTS BETWEEN EACH FOOT AND Ψ VARIABLES.

	$\Psi_{\min}$	$\Psi_{\max}$	Ψ_{avg}
Foot 1	-0.21	-0.38	-0.41
Foot 2	-0.28	0.47	-0.07
Foot 3	-0.35	-0.65	-0.67
Foot 4	0.63	0.45	0.86
Foot$_{avg}$	0.3	-0.15	0.17

Based on Table V, we derived the correlation between the stability margin and the impact force received by each foot, as shown in Table VI. From Table VI, it can be observed that there is no direct linear relationship between the impact force received by each leg and the stability margin. Even though the correlation between Foot 4 and Ψ_{avg} is as high as 0.86, given the symmetric structure of the quadruped robot and considering the correlation values between the other three feet and the stability margin, we cannot solely rely on the high correlation of 0.86 between Foot 4 and Ψ_{avg} to infer a strong relationship between them. Thus, after obtaining the impact force data from the experiments for each foot, we added the data together and took the average to get Foot$_{\text{avg}}$. From the correlation values between Foot$_{\text{avg}}$ and the stability margin in Table VI, it can be concluded that the impact force on the foot is not significantly affected by the gait sequence. This means we cannot identify a relationship between the gait sequence and the magnitude of the impact force received by a foot.

C. Effect of Gait on Robot's Orientations

As depicted in Fig. 10, different gaits have varying effects on the yaw angle. It can be observed from the figure that the influence of different gaits on the robot's yaw angle varies. The correlation between yaw and stability margin values is shown in Table VII.

TABLE VII
CORRELATION BETWEEN YAW AND STABILITY MARGIN.

Stability Margin	**Correlation with Yaw**
$\Psi_{\min}$	-0.769
$\Psi_{\max}$	0.272
Ψ_{avg}	-0.787

From Table VII, it can be observed that the correlation coefficient between the quadruped robot's yaw angle and the minimum stability margin reached -0.769, and with the average stability margin, it reached -0.787. The correlation with the maximum stability margin is only 0.272. In other words, a larger minimum and average stability margin can ensure a smaller yaw angle for the robot.

D. Gait Parameters and Quadruped Stability

Based on the aforementioned analysis, it is evident that due to the varying stability margin values across different gaits, distinct gaits will result in inconsistent stability performance for the robot. As discussed in the experimental analysis above, the gait $\boldsymbol{K}1342$ has an optimal foot-end trajectory relative to other gaits. Furthermore, from the analysis of yaw angle and stability margin, it can be inferred that the robot's yaw angle is closely related to the average stability margin. Hence, once the robot's structural design is finalized and the gait sequence is determined, adjusting the foot distance a can also modify the value of Ψ_{avg}. In practical control, the robot's walking

IEEE Robotics and Automation Letters (RA-L) paper, presented at ICRA 2024, Yokohama, Japan. Cite as RA-L paper.

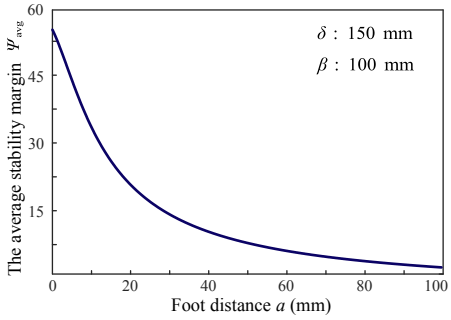

Fig. 11. Relationship curve between average stability margin Ψ_{avg} and foot distance a.

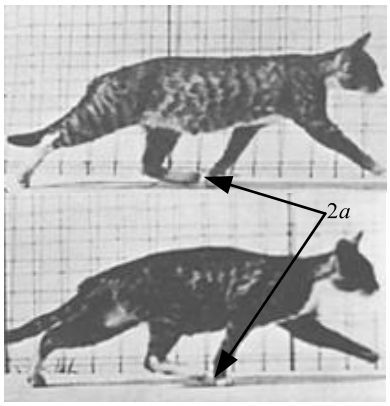

Fig. 12. Catwalk on slow walk [2].

stability can be enhanced by adjusting the foot distance a. The relationship between the average stability margin Ψ_{avg} and the foot distance a is depicted in Fig. 11.

As can be seen from Fig. 11, the smaller the foot distance a of a quadruped robot, the higher its stability. In nature, quadrupeds also try to keep their foot distance as close to 0 as possible when they adopt a crawling gait. The most typical example is the family of cats, whose foot distance is almost equal to 0. This may be one of the reasons why cats have excellent motion stability [31]. Fig. 12 shows the cat's step [2] with a foot distance close to 0. As shown in Fig. 13, when a Bichon Frise dog walks cautiously on ice, it tries to keep its stride distance as close to 0 as possible in order to maintain stability.

Fig. 14 illustrates the influence of body width δ and support distance β on the average stability margin Ψ_{avg} when the foot

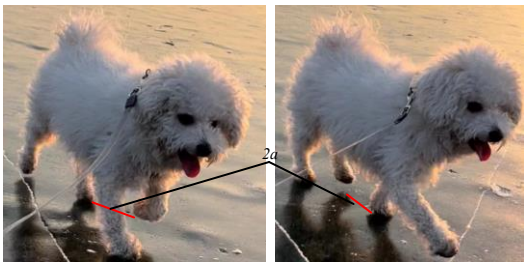

Fig. 13. A Bichon Frise walking on ice.

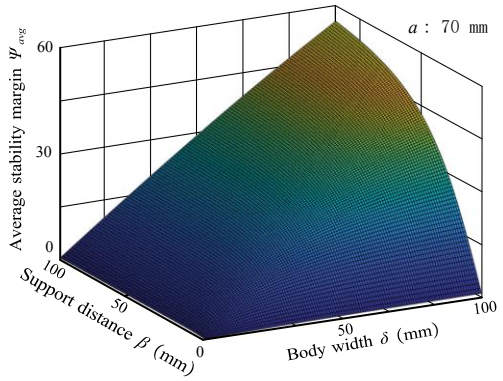

Fig. 14. Influence of body width and support distance on average stability margin.

distance a is fixed. As inferred from Fig. 14, when the foot distance a is determined, the average stability margin Ψ_{avg} increases with an increase in both body width δ and support distance β. However, the average stability margin is more significantly impacted by the body width δ than the support distance β. Hence, during the initial stages of designing a quadruped robot, increasing the body width δ can enhance the overall stability of motion. Additionally, during the motion adjustment phase of quadruped robot design, reducing the foot distance a during gait planning can improve stability.

E. Limitations and Future Work

1) This study is conducted under the assumption of a flat terrain, which limits its applicability to more complex environments. Additionally, it is assumed that when the minimum stability margin of the quadruped robot is greater than zero, the body of the robot remains parallel to the ground.

2) The focus is on static stability metrics, such as the minimum distance from the center of mass, without considering dynamic factors like the velocity of the center of mass.

3) The mass distribution in the robot's legs, a factor potentially impacting stability, is not accounted for.

Future work should aim to address these limitations by exploring more diverse terrains and incorporating dynamic stability metrics.

IV. Conclusion

This study examines the influence of different crawling gait sequences on the stability of quadruped robots. Through theoretical analysis and empirical verification, the following conclusions were drawn:

1) When quadruped robots employ the $\boldsymbol{K}_{1342}$ gait sequence, its minimum stability margin value $\Psi_{min} = 0$ ranks the highest among six gait sequences. Furthermore, the average stability margin $\Psi_{avg} = 2\delta\beta\left(9\delta^2 + (3a+\beta)^2\right)^{-\frac{1}{2}}$ also attains the maximum value amongst all six stability margins. Throughout the entire gait cycle of the $\boldsymbol{K}_{1342}$ sequence, the maximum and minimum support areas, $S_{\Delta max}$ and $S_{\Delta min}$ respectively, are equal, implying less abrupt changes in movement. The study also validated the superior stability of the $\boldsymbol{K}_{1342}$ gait sequence compared to other gait sequences.

2) Empirical observations indicated that when quadruped robots adopt the $\boldsymbol{K}_{1342}$ and $\boldsymbol{K}_{1243}$ gait sequences, their motion curves are more stable. The gait sequences $\boldsymbol{K}_{1432}$, $\boldsymbol{K}_{1234}$, $\boldsymbol{K}_{1324}$, and $\boldsymbol{K}_{1423}$ exhibited deviations from the predetermined trajectory during movement, thereby failing to strictly adhere to control commands. The stability domain of the $\boldsymbol{K}_{1243}$ sequence is small, suggesting a diminished adaptability to unstructured terrain. Consequently, the $\boldsymbol{K}_{1342}$ sequence emerges as the optimal gait sequence for quadruped robots.

3) After adopting a certain gait, the performance of a quadruped robot also correlates with the body width δ, support distance β, and foot distance a. The average stability margin Ψ_{avg} escalates with an increase in the body width δ and support distance β, with a more pronounced impact from the body width δ. When the body width δ and support distance β are set, the average stability margin Ψ_{avg} enlarges with a decrease in foot distance a. The presence of felines with small step distances in nature also underpins this conclusion.

Grounded on screw theory, this study derives the influence of different gait sequences on the stability of quadruped robots, thereby laying a theoretical foundation for future design and stability control of quadruped robots.

ACKNOWLEDGMENTS

This work supported by Research Program supported by National Natural Science Foundation of China (Grant No. 51875495).

REFERENCES

[1] K. D. Rose, *The beginning of the age of mammals*. JHU Press, 2006.
[2] E. Muybridge, *Animals in motion*. Courier Corporation, 2012.
[3] A. Bouman, M. F. Ginting, N. Alatur, M. Palieri, D. D. Fan, T. Touma, T. Pailevanian, S.-K. Kim, K. Otsu, J. Burdick, *et al.*, "Autonomous spot: Long-range autonomous exploration of extreme environments with legged locomotion," in *2020 IEEE/RSJ International Conference on Intelligent Robots and Systems (IROS)*. IEEE, 2020, pp. 2518–2525.
[4] N. Kau, A. Schultz, N. Ferrante, and P. Slade, "Stanford doggo: An open-source, quasi-direct-drive quadruped," in *2019 International Conference on Robotics and Automation (ICRA)*, 2019, pp. 6309–6315.
[5] Q. Shi, J. Gao, S. Wang, X. Quan, G. Jia, Q. Huang, and T. Fukuda, "Development of a small-sized quadruped robotic rat capable of multimodal motions," *IEEE Transactions on Robotics*, vol. 38, no. 5, pp. 3027–3043, 2022.
[6] J. Hooks, M. S. Ahn, J. Yu, X. Zhang, T. Zhu, H. Chae, and D. Hong, "Alphred: A multi-modal operations quadruped robot for package delivery applications," *IEEE Robotics and Automation Letters*, vol. 5, no. 4, pp. 5409–5416, 2020.
[7] C. Semini, N. G. Tsagarakis, E. Guglielmino, M. Focchi, F. Cannella, and D. G. Caldwell, "Design of hyq – a hydraulically and electrically actuated quadruped robot," *Proceedings of the Institution of Mechanical Engineers, Part I: Journal of Systems and Control Engineering*, vol. 225, no. 6, pp. 831–849, 2011. [Online]. Available: https://doi.org/10.1177/0959651811402275
[8] R. B. McGhee and A. A. Frank, "On the stability properties of quadruped creeping gaits," *Mathematical Biosciences*, vol. 3, pp. 331–351, 1968.
[9] E. Garcia, M. A. Jimenez, P. G. De Santos, and M. Armada, "The evolution of robotics research," *IEEE Robotics & Automation Magazine*, vol. 14, no. 1, pp. 90–103, 2007.
[10] A. Gupta, S. Savarese, S. Ganguli, and L. Fei-Fei, "Embodied intelligence via learning and evolution," *Nature communications*, vol. 12, no. 1, p. 5721, 2021.
[11] P. Fankhauser, M. Bjelonic, C. D. Bellicoso, T. Miki, and M. Hutter, "Robust rough-terrain locomotion with a quadrupedal robot," in *2018 IEEE International Conference on Robotics and Automation (ICRA)*. IEEE, 2018, pp. 5761–5768.
[12] D. J. Hyun, S. Seok, J. Lee, and S. Kim, "High speed trot-running: Implementation of a hierarchical controller using proprioceptive impedance control on the mit cheetah," *The International Journal of Robotics Research*, vol. 33, no. 11, pp. 1417–1445, 2014.
[13] C. D. Bellicoso, F. Jenelten, C. Gehring, and M. Hutter, "Dynamic locomotion through online nonlinear motion optimization for quadrupedal robots," *IEEE Robotics and Automation Letters*, vol. 3, no. 3, pp. 2261–2268, 2018.
[14] A. W. Winkler, F. Farshidian, M. Neunert, D. Pardo, and J. Buchli, "Online walking motion and foothold optimization for quadruped locomotion," in *2017 IEEE International Conference on Robotics and Automation (ICRA)*. IEEE, 2017, pp. 5308–5313.
[15] S. Yuan, Y. Zhou, and C. Luo, "Crawling gait planning based on foot trajectory optimization for quadruped robot," in *2019 IEEE International Conference on Mechatronics and Automation (ICMA)*, 2019, pp. 1490–1495.
[16] M. Kalakrishnan, J. Buchli, P. Pastor, M. Mistry, and S. Schaal, "Learning, planning, and control for quadruped locomotion over challenging terrain," *The International Journal of Robotics Research*, vol. 30, no. 2, pp. 236–258, 2011.
[17] Q. Hao, Z. Wang, J. Wang, and G. Chen, "Stability-guaranteed and high terrain adaptability static gait for quadruped robots," *Sensors*, vol. 20, no. 17, p. 4911, 2020.
[18] F. A.Raheem and M. K. Flayyih, "Quadruped robot creeping gait stability analysis and optimization using pso," in *2017 Second Al-Sadiq International Conference on Multidisciplinary in IT and Communication Science and Applications (AIC-MITCSA)*, 2017, pp. 79–84.
[19] T. Srinivas, A. K. K. Madhusudhan, L. Manohar, N. M. Stephen Pushpagiri, K. C. Ramanathan, M. Janardhanan, and I. Nielsen, "Valkyrie—design and development of gaits for quadruped robot using particle swarm optimization," *Applied Sciences*, vol. 11, no. 16, p. 7458, 2021.
[20] Y. J. Lee and Z. Bien, "A hierarchical strategy for planning crab gaits of a quadruped walking robot," *Robotica*, vol. 12, no. 1, p. 23–31, 1994.
[21] D. Belter and P. Skrzypczyński, "Rough terrain mapping and classification for foothold selection in a walking robot," *Journal of Field Robotics*, vol. 28, no. 4, pp. 497–528, 2011.
[22] O. A. V. Magana, V. Barasuol, M. Camurri, L. Franceschi, M. Focchi, M. Pontil, D. G. Caldwell, and C. Semini, "Fast and continuous foothold adaptation for dynamic locomotion through cnns," *IEEE Robotics and Automation Letters*, vol. 4, no. 2, pp. 2140–2147, 2019.
[23] D. Belter, J. Bednarek, H.-C. Lin, G. Xin, and M. Mistry, "Single-shot foothold selection and constraint evaluation for quadruped locomotion," in *2019 International Conference on Robotics and Automation (ICRA)*. IEEE, 2019, pp. 7441–7447.
[24] L. Chen, S. Ye, C. Sun, A. Zhang, G. Deng, T. Liao, and J. Sun, "Cnns based foothold selection for energy-efficient quadruped locomotion over rough terrains," in *2019 IEEE International Conference on Robotics and Biomimetics (ROBIO)*. IEEE, 2019, pp. 1115–1120.
[25] M. Kalakrishnan, J. Buchli, P. Pastor, and S. Schaal, "Learning locomotion over rough terrain using terrain templates," in *2009 IEEE/RSJ International Conference on Intelligent Robots and Systems*, 2009, pp. 167–172.
[26] T. Akbas, S. E. Eskimez, S. Ozel, O. K. Adak, K. C. Fidan, and K. Erbatur, "Zero moment point based pace reference generation for quadruped robots via preview control," in *2012 12th IEEE International Workshop on Advanced Motion Control (AMC)*. IEEE, 2012, pp. 1–7.
[27] R. Orsolino, M. FOCCHI, D. G. CALDWELL, and C. SEMINI, "A combined limit cycle-zero moment point based approach for omnidirectional quadrupedal bounding," in *Human-Centric Robotics: Proceedings of CLAWAR 2017: 20th International Conference on Climbing and Walking Robots and the Support Technologies for Mobile Machines*. World Scientific, 2018, pp. 407–414.
[28] B. Katz, J. D. Carlo, and S. Kim, "Mini cheetah: A platform for pushing the limits of dynamic quadruped control," in *2019 International Conference on Robotics and Automation (ICRA)*, 2019, pp. 6295–6301.
[29] B. Jin, S. Ye, J. Su, and J. Luo, "Unknown payload adaptive control for quadruped locomotion with proprioceptive linear legs," *IEEE/ASME Transactions on Mechatronics*, vol. 27, no. 4, pp. 1891–1899, 2022.
[30] H. Chen, Z. Hong, S. Yang, P. M. Wensing, and W. Zhang, "Quadruped capturability and push recovery via a switched-systems characterization of dynamic balance," *IEEE Transactions on Robotics*, pp. 1–20, 2023.
[31] J. M. Macpherson and J. Fung, "Weight support and balance during perturbed stance in the chronic spinal cat," *Journal of Neurophysiology*, vol. 82, no. 6, pp. 3066–3081, 1999.